Vol.2, No.9, 968-978 (2010)
http://dx.doi.org/10.4236/ns.2010.29118

Natural Science

Thermal buckling analysis of ceramic-metal functionally graded plates

Ashraf M. Zenkour[1,2]*, Daoud S. Mashat[1]

[1]Department of Mathematics, Faculty of Science, King AbdulAziz University, Jeddah, Saudi Arabia;
*Corresponding Author: zenkour@kau.edu.sa
[2]Department of Mathematics, Faculty of Science, Kafrelsheikh University, Kafr El-Sheikh, Egypt

Received 7 March 2010; revised 20 April 2010; accepted 26 April 2010.

ABSTRACT

Thermal buckling response of functionally graded plates is presented in this paper using sinusoidal shear deformation plate theory (SPT). The material properties of the plate are assumed to vary according to a power law form in the thickness direction. Equilibrium and stability equations are derived based on the SPT. The non-linear governing equations are solved for plates subjected to simply supported boundary conditions. The buckling analysis of a functionally graded plate under various types of thermal loads is carried out. The influences of many plate parameters on buckling temperature difference will be investigated. Numerical results are presented for the SPT, demonstrating its importance and accuracy in comparison to other theories.

Keywords: Thermal Buckling; Non-Linear Strains; Functionally Graded Material; Sinusoidal Plate Theory; Thermal Load

1. INTRODUCTION

The rapid development of composite materials and structures in recent years has drawn increased attention from many engineers and researchers. These materials are broadly used in aerospace, mechanical, nuclear, marine, and structural engineering. In conventional laminated composite structures, homogeneous elastic laminas are bonded together to obtain enhanced mechanical and thermal properties. However, the abrupt change in material properties across the interface between different materials can result in large inter-laminar stresses leading to delimitation, cracking, and other damage mechanisms which result from the abrupt change of the mechanical properties at the interface between the layers. To remedy such defects, functionally graded materials (FGMs), within which material properties vary continuously, have been proposed.

The concept of FGM was proposed in 1984 by a group of materials scientists, in Sendai, Japan, for thermal barriers or heat shielding properties. Initially FGM was designed as a thermal barrier material for aerospace application and fusion reactors. Later on FGM was developed for the military, automotive, biomedical and semiconductor industries, and as a general structural element in high thermal environments. FGM is one of the advanced high temperature materials capable of withstanding extreme temperature environments. FGMs are composite and microscopically heterogeneous in which the mechanical properties vary smoothly and continuously from one surface to the other. This is achieved by gradually varying the volume fraction of the constituent materials. Typically, these materials are made from a mixture of ceramics and metal or a combination of different materials. The ceramic constituent of the material provides the high-temperature resistance due to its low thermal conductivity and protects the metal from oxidation. The ductile metal constituent, on the other hand, prevents fracture caused by stresses due to high-temperature gradient in a very short period of time. Further, a mixture of a ceramic and a metal with a continuously varying volume fraction can be easily manufactured [1-4].

A comprehensive work on the FGMs was presented in the literature. The response of FG ceramic-metal plates has been investigated by Praveen and Reddy [5] using a plate finite element. They investigated the static and dynamic thermoelastic responses of the FGMs by varying the volume fraction using a simple power law distribution. Reddy [6] developed the Navier's solutions for FG plates using the third-order shear deformation plate theory (TSDT) and an associated finite element model. Amini *et al.* [7] described a method for three-dimensional free vibration analysis of rectangular FGM plates

resting on an elastic foundation using Chebyshev polynomials and Ritz's method. This analysis has been based on a linear, small-strain, three-dimensional elasticity theory. Analysis of FG plates under static and dynamic loads has been presented by Sladek *et al.* [8] using the meshless local Petrov-Galerkin method and Reissner-Mindlin theory to describe the plate bending problem. Kim *et al.* [9] investigated finite element computation of fracture parameters in FGM assemblages of arbitrary geometry with stationary cracks. In Altenbach and Eremeyev [10], a viscoelastic FG polymer foam has been studied using a new plate theory based on the direct approach. The large deflection response of simply supported rectangular FG plates under normal pressure loading has been analyzed by Ovesy and Ghannadpour [11] using a finite strip method. In Han [12], a numerical method was proposed for analyzing transient waves in plates of FGM excited by impact loads. The bending problem of transverse load acting on FGM rectangular plate using both two-dimensional trigonometric and three-dimensional elasticity solutions was investigated by Zenkour [13]. Zenkour [14,15] studied the bending response, buckling and free vibration of simply supported FG sandwich plate using the SPT. Zenkour [16] presented the derivation of equations for free vibration of FG plates expressing the displacement components by trigonometric series representation through the plate thickness. Other researches into FGMs have included the nonlinear analysis of FG plates [17], large deformation analysis of FG shells [18], static and vibration analysis of FG beams [19,20].

In view of the advantages of FGMs, a number of investigations dealing with thermal buckling had been published in the scientific literature. In recent years, the mechanical and thermal buckling analysis of FG ceramic-metal plates has been presented by Zhao *et al*. [21] using the first-order shear deformation plate theory, in conjunction with the Ritz method. A two-dimensional global higher-order deformation theory has been employed by Matsunaga [22] for thermal buckling of plates made of FGMs. Morimoto *et al.* [23] presented the thermal buckling analysis of FG rectangular plates subjected to partial heating in a plane and uniform temperature rise through its thickness. In Ref. [24], Shariat and Eslami presented the thermal buckling analysis of rectangular FG plates with geometrical imperfections using the classical plate theory to derive the equilibrium, stability, and compatibility equations of an imperfect FGM. Thermal buckling of rectangular and circular plates compose of FGM was also studied based on the first- and higher-order shear deformation plate theory [25-27].

Various plate theories, depending upon the through-thickness displacement pattern considered, have been used to determine thermal buckling loads of composite plates. The classical plate theory [24], which is based on Kirchhoff's hypothesis, overestimates the thermal buckling load when applied to even moderately thick plates. This is particularly true for composite plates in which transverse shear moduli are small in comparison to the in-plane Young's moduli [28]. In such cases, it becomes necessary to take into account shear deformation effects. Thus, various improved plate theories such as first-order shear deformation [25,26], higher order shear deformation [5,6] and sinusoidal shear deformation [13-16,29-31] plate theories have been developed to predict the behavior of plates with thickness shear deformation. In this article, thermal buckling analysis of rectangular FG ceramic-metal plates is investigated. The material properties of the FG plates are assumed to vary continuously through the thickness, according to a simple power law distribution of the volume fraction of the constituents. The SPT is used to obtain the buckling of the plate under different types of thermal loads. The thermal loads are assumed to be uniform, linear and non-linear distribution through the thickness. Additional numerical results are presented for FGM plates that show the effects of various parameters on thermal buckling response.

2. MATHEMATICAL MODEL

Consider a rectangular plate of length a, width b and thickness h made of FGM. The plate is subjected to a thermal load $T(x,y,z)$. The material properties of the FGM plate, such as Young's modulus E and thermal expansion coefficients α are assumed to be functions of the volume fraction of the constituent materials. The FGM plate is supported at four edges defined in the (x,y,z) coordinate system with x- and y-axes located in the middle plane $(z=0)$ and its origin placed at the corner of the plate.

The modulus of elasticity E, the coefficient of thermal expansion α and Poisson's ratio ν are assumed as [5]

$$\begin{aligned} &E(z)=E_{\mathrm{m}}+E_{\mathrm{cm}}V^{k},\\ &\alpha(z)=\alpha_{\mathrm{m}}+\alpha_{\mathrm{cm}}V^{k},\ \nu(z)=\nu_{0}, \end{aligned} \tag{1}$$

where

$$\begin{aligned} &E_{\mathrm{cm}}=E_{\mathrm{c}}-E_{\mathrm{m}},\\ &\alpha_{\mathrm{cm}}=\alpha_{\mathrm{c}}-\alpha_{\mathrm{m}},\\ &V=\left(\frac{z}{h}+\frac{1}{2}\right), \end{aligned} \tag{2}$$

and E_{m} and α_{m} denote the elastic moduli and the coefficient of thermal expansion of metal; E_{c} and α_{c} denote the elastic moduli and the coefficient of thermal

expansion of ceramic, and k is the volume fraction exponent. The value of k equal to zero represents a fully ceramic plate. The above power law assumption reflects a simple rule of mixtures used to obtain the effective properties of the ceramic-metal plate. The rule of mixtures applies only to the thickness direction. The density of the plate varies according to the power law, and the power law exponent may be varied to obtain different distributions of the component materials through the thickness of plate. Note that the volume fraction of the metal is high near the bottom surface of the plate, and that of ceramic high near the top surface. In addition, **Eq.1** indicates that the bottom surface of the plate $(z=-h/2)$ is metal-rich whereas the top surface $(z=h/2)$ of the plate is ceramic-rich. For simplicity, ν is assumed constant across the plate thickness.

The displacements of a material point located at (x, y, z) in the FGM plate might better be illustrated as [29, 30]:

$$\left.\begin{aligned} u_1(x,y,z) &= u - z\frac{\partial w}{\partial x} + \Psi(z)\varphi_1, \\ u_2(x,y,z) &= v - z\frac{\partial w}{\partial y} + \Psi(z)\varphi_2, \\ u_3(x,y,z) &= w, \end{aligned}\right\} \tag{3}$$

where u, v and w are the displacements of the middle surface along the axes x, y and z, respectively, and φ_1 and φ_2 are the rotations about the y and x-axes and account for the effect of transverse shear. The coefficient of φ_1 or φ_2 which is given by $\Psi(z)$ should be odd function of z. All of the generalized displacements $(u,v,w,\varphi_1,\varphi_2)$ are functions of the (x, y). The displacement of the classical thin plate theory (CPT) can easily be obtained by setting $\Psi(z)=0$. The displacements of the first-order shear deformation plate theory (FPT) are obtained by setting $\Psi(z)=z$. In addition, the higher-order shear deformation plate theory (HPT) [6] is obtained by setting

$$\Psi(z) = z\left[1-\frac{4}{3}\left(\frac{z}{h}\right)^2\right]. \tag{4}$$

Also, the SPT is obtained by setting [14,15]:

$$\Psi(z) = \frac{h}{\pi}\sin\left(\frac{\pi z}{h}\right). \tag{5}$$

Note that the present SPT, as well as HPT, is simplified by enforcing traction-free boundary conditions at the plate faces. The SPT accounts according to a cosine-law distribution of the transverse shear deformation through the thickness of the FGM plate. The SPT, HPT and FPT contain the same number of dependent unknowns. No transversal shear correction factors are needed for both SPT and HPT because a correct representation of the transversal shearing strain is given.

The non-linear strain components ε_{ij} compatible with the displacement field in **Eq.3** are

$$\begin{Bmatrix} \varepsilon_{11} \\ \varepsilon_{22} \\ \varepsilon_{12} \end{Bmatrix} = \begin{Bmatrix} \varepsilon_{11}^0 \\ \varepsilon_{22}^0 \\ \varepsilon_{12}^0 \end{Bmatrix} + z\begin{Bmatrix} \kappa_{11} \\ \kappa_{22} \\ \kappa_{12} \end{Bmatrix} + \Psi(z)\begin{Bmatrix} \eta_{11} \\ \eta_{22} \\ \eta_{12} \end{Bmatrix}, \tag{6}$$

$$\varepsilon_{33} = 0, \quad \begin{Bmatrix} \varepsilon_{23} \\ \varepsilon_{13} \end{Bmatrix} = \Psi(z)_{,3}\begin{Bmatrix} \varepsilon_{23}^0 \\ \varepsilon_{13}^0 \end{Bmatrix}, \tag{7}$$

where

$$\begin{aligned} &\varepsilon_{11}^0 = u_{,1} + \tfrac{1}{2}w_{,1}^2,\ \varepsilon_{22}^0 = v_{,2} + \frac{1}{2}w_{,2}^2,\ \varepsilon_{23}^0 = \varphi_2,\ \varepsilon_{13}^0 = \varphi_1, \\ &\varepsilon_{12}^0 = v_{,1} + u_{,2} + w_{,1}w_{,2}, \\ &\kappa_{11} = -w_{,11},\ \kappa_{22} = -w_{,22},\ \kappa_{12} = -2w_{,12}, \\ &\eta_{11} = \varphi_{1,1},\ \eta_{22} = \varphi_{2,2},\ \eta_{12} = \varphi_{2,1} + \varphi_{1,2}. \end{aligned} \tag{8}$$

The stress-strain relations for the FGM plate are given by

$$\begin{Bmatrix} \sigma_{11} \\ \sigma_{22} \end{Bmatrix} = \frac{E(z)}{1-\nu^2}\begin{bmatrix} 1 & \nu \\ \nu & 1 \end{bmatrix}\begin{Bmatrix} \varepsilon_{11}-\alpha T \\ \varepsilon_{22}-\alpha T \end{Bmatrix}, \tag{9}$$

$$\{\sigma_{23},\sigma_{13},\sigma_{12}\} = \frac{E(z)}{2(1+\nu)}\{\varepsilon_{23},\varepsilon_{13},\varepsilon_{12}\},$$

where $T(x,y,z)$ is the temperature rise through the thickness.

The stress and moment resultants of the FGM plate can be obtained by integrating **Eq.9** over the thickness, and are written as

$$\begin{Bmatrix} N_i \\ M_i \\ S_i \end{Bmatrix} = \frac{1}{1-\nu^2}\begin{bmatrix} A_k & B_k & C_k \\ B_k & D_k & F_k \\ C_k & F_k & G_k \end{bmatrix}\begin{Bmatrix} \bar{\varepsilon}_i^0 \\ \bar{\kappa}_i \\ \bar{\eta}_i \end{Bmatrix} + \frac{1}{\nu-1}\begin{bmatrix} A_T \\ B_T \\ C_T \end{bmatrix}, \tag{10}$$

$$\begin{Bmatrix} N_{12} \\ M_{12} \\ S_{12} \end{Bmatrix} = \frac{1}{2(1+\nu)}\begin{bmatrix} A_k & B_k & C_k \\ B_k & D_k & F_k \\ C_k & F_k & G_k \end{bmatrix}\begin{Bmatrix} \varepsilon_{12}^0 \\ \kappa_{12} \\ \eta_{12} \end{Bmatrix}, \tag{11}$$

and

$$\begin{Bmatrix} Q_{13} \\ Q_{23} \end{Bmatrix} = \frac{H_k}{2(1+\nu)} \begin{Bmatrix} \varepsilon_{13}^0 \\ \varepsilon_{23}^0 \end{Bmatrix}, \tag{12}$$

where $i = 1, 2$ and

$$\begin{aligned} \bar{\varepsilon}_1^0 &= \varepsilon_{11}^0 + \nu\varepsilon_{22}^0, & \bar{\varepsilon}_2^0 &= \varepsilon_{22}^0 + \nu\varepsilon_{11}^0, \\ \bar{\kappa}_1 &= \kappa_{11} + \nu\kappa_{22}, & \bar{\kappa}_2 &= \kappa_{22} + \nu\kappa_{11}, \\ \bar{\eta}_1 &= \eta_{11} + \nu\eta_{22}, & \bar{\eta}_2 &= \eta_{22} + \nu\eta_{11}. \end{aligned} \tag{13}$$

In **Eqs.10-12,** $N_1, N_2,$ and N_{12} and $M_1, M_2,$ and M_{12} are the basic components of stress resultants and stress couples; $S_1, S_2,$ and S_{12} are additional stress couples associated with the transversal shear effects; and Q_{13} and Q_{23} are transversal shear stress resultants. The coefficients $A_k, B_k, C_k, \ldots$ etc. are defined by

$$\begin{aligned} \{A_k, B_k, D_k\} &= \int_{-h/2}^{+h/2} E(z)\{1, z, z^2\}\,\mathrm{d}z, \\ \{C_k, F_k, G_k\} &= \int_{-h/2}^{+h/2} \Psi(z)E(z)\{1, z, \Psi(z)\}\,\mathrm{d}z, \\ \{A_T, B_T, C_T\} &= \int_{-h/2}^{+h/2} \alpha(z)E(z)T(x, y, z)\{1, z, \Psi(z)\}\,\mathrm{d}z, \\ H_k &= \int_{-h/2}^{+h/2} E(z)(\Psi(z)_{,3})^2\,\mathrm{d}z. \end{aligned} \tag{14}$$

3. EQUILIBRIUM AND STABILITY EQUATIONS

The total potential energy of a plate subjected to thermal loads is defined as [27]

$$V = U_m + U_b + U_c + U_T, \tag{15}$$

where U_m, U_b, U_c and U_T are membrane strain energy, bending strain energy, coupled strain energy and thermal strain energy. The strain energy for FGM plate based on the SPT is defined as given below in **Eq.16**.

The equilibrium and stability equations of FGM plates may be derived by the variational approach. The expansion of V about the equilibrium state by the Taylor series is

$$\Delta V = \delta V + \tfrac{1}{2!}\delta^2 V + \tfrac{1}{3!}\delta^3 V + \ldots\,. \tag{17}$$

The governing equations of equilibrium can be derived by using the first variation δV. The non-linear equilibrium equations associated with the present SPT are

$$\begin{gathered} N_{1,1} + N_{12,2} = 0, \\ N_{12,1} + N_{2,2} = 0, \\ M_{1,11} + 2M_{12,12} + M_{2,22} + N_1 w_{,11} + N_2 w_{,22} + 2N_{12} w_{,12} = 0, \\ S_{1,1} + S_{12,2} - Q_{13} = 0, \\ S_{12,1} + S_{2,2} - Q_{23} = 0. \end{gathered} \tag{18}$$

To establish the stability equations, the condition $\delta^2 V = 0$ used to derive the stability equations of many practical plate buckling problems is also used here. The external load acting on the original configuration is considered to be the critical buckling temperature if the above equation $(\delta^2 V = 0)$ is satisfied. Assuming that the state of stable equilibrium of a general plate under thermal load may be designated by $u^0, v^0, w^0, \phi_1^0, \phi_2^0$. The displacements of the neighboring state are

$$\begin{aligned} u &= u^0 + u^1, \quad \varphi_1 = \varphi_1^0 + \varphi_1^1, \\ v &= v^0 + v^1, \quad \varphi_2 = \varphi_2^0 + \varphi_2^1, \\ w &= w^0 + w^1, \end{aligned} \tag{19}$$

where $u^1, v^1, w^1, \varphi_1^1$ and φ_2^1 are arbitrarily small increment of displacements. The stability equations are represented by using the above total displacement given in **Eq.19** in the equation $\delta^2 V = 0$ and collecting the second-order terms. They read

$$\begin{gathered} N_{1,1}^1 + N_{12,2}^1 = 0, \\ N_{12,1}^1 + N_{2,2}^1 = 0, \\ M_{1,11}^1 + 2M_{12,12}^1 + M_{2,22}^1 + N_1^0 w_{,11}^1 + N_2^0 w_{,22}^1 + 2N_{12}^0 w_{,12}^1 = 0, \\ S_{1,1}^1 + S_{12,2}^1 - Q_{13}^1 = 0, \\ S_{12,1}^1 + S_{2,2}^1 - Q_{23}^1 = 0, \end{gathered} \tag{20}$$

where the superscript 1 refers to the state of stability and the superscript 0 refers to the state of equilibrium conditions. The terms N_1^0, N_2^0 and N_{12}^0 are the pre-buckling force resultants obtained as

$$N_1^0 = \frac{A_T}{\nu - 1}, \; N_1^0 = \frac{A_T}{\nu - 1}, \; N_{12}^0 = 0\,. \tag{21}$$

4. EXACT SOLUTIONS FOR THERMAL BUCKLING OF FGM PLATES

Rectangular plates are generally classified in accordance

$$V = \frac{1}{2}\iiint_{\mathrm{v}} \left[\sigma_{11}\left(\varepsilon_{11} - \alpha T\right) + \sigma_{22}\left(\varepsilon_{22} - \alpha T\right) + \sigma_{12}\varepsilon_{12} + \sigma_{23}\varepsilon_{23} + \sigma_{13}\varepsilon_{13}\right]\mathrm{d}\,\mathrm{v}. \tag{16}$$

with the type support used in the absent of the body forces and lateral loads except the external temperature load. The following boundary conditions are imposed at the side edges

$$\begin{aligned} &v^1 = w^1 = \varphi_2^1 = N_1^1 = M_1^1 = S_1^1 = 0 \text{ at } x = 0,\ a, \\ &u^1 = w^1 = \varphi_1^1 = N_2^1 = M_2^1 = S_2^1 = 0 \text{ at } y = 0,\ b, \end{aligned} \tag{22}$$

Following Navier solution procedure, we assume the following solution form for $(u^1, v^1, w^1, \varphi_1^1, \varphi_2^1)$ that satisfies the simply-supported boundary conditions,

$$\begin{Bmatrix} u^1 \\ v^1 \\ w^1 \\ \varphi_1^1 \\ \varphi_2^1 \end{Bmatrix} = \sum_{m,n=1}^{\infty} \begin{Bmatrix} U_{mn}^1 \cos(\lambda x)\sin(\mu y) \\ V_{mn}^1 \sin(\lambda x)\cos(\mu y) \\ W_{mn}^1 \sin(\lambda x)\sin(\mu y) \\ X_{mn}^1 \cos(\lambda x)\sin(\mu y) \\ Y_{mn}^1 \sin(\lambda x)\cos(\mu y) \end{Bmatrix}, \tag{23}$$

where $\lambda = m\pi/a$, $\mu = n\pi/b$; m and n are mode numbers; $U_{mn}^1, V_{mn}^1, W_{mn}^1, X_{mn}^1$, and Y_{mn}^1 are arbitrary parameters to be determined subjected to the condition that the solution in **Eq.23** satisfies the conditions in **Eq.22**. Substituting **Eq.23** into **Eq.20**, one obtains

$$[L]\{\Omega\} = 0, \tag{24}$$

where $\{\Omega\}$ denotes the column

$$\{\Omega\}^t = \{U_{mn}^1, V_{mn}^1, W_{mn}^1, X_{mn}^1, Y_{mn}^1\}, \tag{25}$$

and elements $L_{rs} = L_{sr}$ of the coefficient matrix $[L]$ are given by:

$$\begin{aligned} L_{11} &= -A_k[2\lambda^2 + (1-\nu)\mu^2], \\ L_{12} &= -\lambda\mu A_k(1+\nu), \\ L_{13} &= 2\lambda B_k(\lambda^2 + \mu^2), \\ L_{14} &= -C_k[2\lambda^2 + (1-\nu)\mu^2], \\ L_{15} &= -\lambda\mu C_k(1+\nu), \\ L_{22} &= -A_k[(1-\nu)\lambda^2 + 2\mu^2], \\ L_{23} &= 2\mu B_k(\lambda^2 + \mu^2), \\ L_{24} &= L_{15}, \\ L_{25} &= -C_k[(1-\nu)\lambda^2 + 2\mu^2], \\ L_{33} &= -2(\lambda^2 + \mu^2)[D_k(\lambda^2 + \mu^2) - A_T(1+\nu)], \\ L_{34} &= 2\lambda F_k(\lambda^2 + \mu^2), \\ L_{35} &= 2\mu F_k(\lambda^2 + \mu^2), \\ L_{44} &= -G_k[2\lambda^2 + (1-\nu)\mu^2] - H_k(1-\nu), \\ L_{45} &= -\lambda\mu G_k(1+\nu), \\ L_{55} &= -G_k[(1-\nu)\lambda^2 + 2\mu^2] - H_k(1-\nu). \end{aligned} \tag{26}$$

For non-trivial solutions of **Eq.24**, the determinant $|L|$ should be zero. This equation $(|L| = 0)$ is stated for the determination of the lowest critical load. In the following, the solutions of the equation $|L| = 0$ for different types of thermal loading conditions are presented. The plate is assumed simply supported in bending and rigidly fixed in extension. The temperature change is varied only in the thickness direction.

4.1. Thermal Buckling for FGM Plates under Uniform Temperature Rise

The initial uniform temperature of the plate is assumed to be T_i. The temperature is uniformly raised to a final value T_f in which the plate buckles. The temperature change is $\Delta T = T_f - T_i$. Substituting **Eq.26** into the equation $|L| = 0$, the buckling temperature change using the shear deformation theories is obtained as

$$\Delta T = \frac{\pi^2(n^2s^2 + m^2)[\bar{P}_1 a^2(1-\nu) + \bar{P}_2\pi^2(n^2s^2 + m^2)]}{a^2 A_{T1}(1+\nu)[P_1 a^2(1-\nu) + P_2\pi^2(n^2s^2 + m^2)]}, \tag{27}$$

where

$$\begin{aligned} &P_1 = A_k H_k,\ P_2 = 2(A_k G_k - C_k^2), \\ &\bar{P}_1 = P_1 D_k - B_k^2 H_k, \\ &\bar{P}_2 = P_2 D_k - 2A_k F_k^2 - 2B_k(B_k G_k - 2F_k C_k), \\ &A_{T1} = \int_{-h/2}^{+h/2} \alpha(z)E(z)\,\mathrm{d}z,\ s = a/b. \end{aligned} \tag{28}$$

The critical buckling temperature change T_{cr}, is the smallest value of ΔT which is obtained when m =1 and n = 1. Therefore,

$$T_{cr} = \frac{\pi^2(s^2+1)[\bar{P}_1 a^2(1-\nu) + \bar{P}_2\pi^2(s^2+1)]}{a^2 A_{T1}(1+\nu)[P_1 a^2(1-\nu) + P_2\pi^2(s^2+1)]}. \tag{29}$$

For the classical plate theory, the critical buckling temperature difference T_{cr} is given as

$$T_{cr} = \frac{\pi^2(s^2+1)(A_k D_k - B_k)}{a^2 A_k A_{T1}(1+\nu)}. \tag{30}$$

4.2. Thermal Buckling for FGM Plates Subjected to a Graded Temperature Change across the Thickness

For an FG plate, the temperature change is not uniform. The temperature varies according to the power law variation. Usually, the temperature rises much higher at

the ceramic side than that in the metal side of the plate. In this case, the temperature through the thickness is given by

$$T(z) = \Delta T V^{\beta} + T_{\mathrm{m}}, \tag{31}$$

where T_{m} is the temperature of the bottom surface which is metal-rich and β is the power law exponent ($0 < \beta < \infty$).

Similar to the previous loading case, solving the equation $|L| = 0$, the buckling temperature difference $\Delta T = T(h/2) - T(-h/2)$ using the shear deformation plate theories can be determined, and then we can obtain the critical buckling T_{cr} as

$$T_{cr} = \frac{\pi^2 (s^2+1)[\bar{P}_1 a^2 (1-\nu) + \bar{P}_2 \pi^2 (s^2+1)]}{a^2 A_{T2}(1+\nu)[P_1 a^2 (1-\nu) + P_2 \pi^2 (s^2+1)]} - \frac{T_m A_{T1}}{A_{T2}}, \tag{32}$$

where

$$A_{T2} = \int_{-h/2}^{+h/2} \alpha(z) V^{\beta} E(z)\, \mathrm{d}z. \tag{33}$$

Also, the critical buckling temperature difference T_{cr} for the classical plate theory, is deduced as

$$T_{cr} = \frac{\pi^2 (s^2+1)(A_k D_k - B_k)}{a^2 A_k A_{T2}(1+\nu)} - \frac{T_m A_{T1}}{A_{T2}}. \tag{34}$$

Note that the value of β equal to unity represents a linear temperature change across the thickness. While the value of β excluding unity represents a non-linear temperature change through the thickness.

5. RESULTS AND DISCUSSION

The general approach outlined in the previous sections for the thermal buckling analysis of the homogeneous and FGM plates under uniform, linear and non-linear temperature rises through the thickness is illustrated in this section using the SPT. The correlation between the present theory and different higher- and first-order shear deformation theories and classical plate theory is established. To illustrate the proposed method, a ceramic-metal FG plate is considered. The combination of materials consists of aluminum and alumina. The Young's modulus and the coefficient of thermal expansion for alumina are $E_{\mathrm{c}} = 380$ GPa, $\alpha_{\mathrm{c}} = 7.4\times10^{-6}/^{\circ}\mathrm{C}$, and for aluminum are $E_{\mathrm{m}} = 70$ GPa, $\alpha_{\mathrm{m}} = 23\times10^{-6}/^{\circ}\mathrm{C}$, respectively. Note that, Poisson's ratio is selected constant for both aluminum and alumina and it equal to 0.3. The shear correction factor for FPT is set equal to 5/6. For the linear and non-linear temperature rises through the thickness, the temperature rises $5^{\circ}\mathrm{C}$ in the metal-rich surface of the plate (*i.e.* $T_{\mathrm{m}} = 5^{\circ}\mathrm{C}$). We will assume in all analyzed cases (unless otherwise stated) that $a/b = 2$, $a/h = 10$, and $\beta = 3$.

Numerical results of the present investigation are given in **Tables 1-4** and **Figures 1-4**. In **Tables 1** and **2**, the side to thickness ratio of the plate is set as $a/h = 100$. In these tables the critical buckling temperature difference T_{cr} of the plate under uniform and linear temperature rises is shown for different values of the power law index *k* using various plate theories. The results obtained as per the present HPT and CPT are compared with the corresponding ones presented by Javaheri and Eslami [32]. Excellent agreement is achieved between the two solutions. It is seen that, for all theories, the critical temperature difference increases monotonically as the aspect ratio a/b increases. Moreover, the critical buckling T_{cr} decreases until it reaches minimum values and then increases as the values of the volume fraction exponent *k* increases. **Tables 3** and **4** exhibit the critical temperature difference $t_{cr} = 10^{-3} T_{cr}$ for different values of the aspect ratio a/b, the temperature exponent β and the power law index k under non-linear temperature loads at $a/h = 10$ and 5, respectively. The nonlinearity temperature exponent β is taken here as 2, 5 and 10. The effect of a/b on the critical buckling t_{cr} is similar to that in the case of uniform and linear temperature difference across the thickness. As the power law index k increases, the critical buckling t_{cr} decreases to reach lowest values and then increases excluding t_{cr} of the rectangular plates for $\beta = 10$. Also, it is noticed that t_{cr} increases as the nonlinearity index β increases. In general, the values of the critical temperature difference calculated by using the shear deformation theories are lower than those calculated by using the classical plate theory, indicating the shear deformation effect. The SPT without using any shear correction factor gives results very close to HPT and closer than those obtained using FPT.

The critical buckling temperature difference t_{cr} of the ceramic-metal FG rectangular plate ($k = 5$) versus the side-to-thickness ratio a/h calculated by all theories under a uniform, linear and non-linear temperature load are shown in **Figure 1**. For plates with small a/h ratio, very large differences between the results of both SPT and HPT and those of both FPT and CPT are observed. Moreover, the differences between the higher-order shear deformation theories (SPT and HPT) and FPT are lower than those between any of them and CPT. However, for a large value of the side-to-thickness ratio the difference between the values predicted by the shear deformation theories and CPT is low significant because the plate is essentially thin. Because of permitting shear deformation in SPT, HPT and FPT, the plate becomes more flexible and thus the critical buckling temperatures calculated by these theories are smaller than those cal-

Table 1. Critical buckling temperature change T_{cr} of FGM plate under uniform temperature rise for different values of power law index k and aspect ratio a/b.

k	Theory	$a/b=1$	$a/b=2$	$a/b=3$	$a/b=4$	$a/b=5$
0	SPT	17.0894	42.6876	85.2554	144.6500	220.6729
	HPT	17.0894 (17.088)	42.6875 (42.688)	85.2551 (85.252)	144.6490 (144.648)	220.6706 (220.667)
	FPT	17.0894	42.6875	85.2551	144.6489	220.6704
	CPT	17.0991 (17.099)	42.7477 (42.747)	85.4955 (85.495)	145.3424 (145.342)	222.2883 (222.288)
1	SPT	7.9400	19.8359	39.6249	67.2510	102.6365
	HPT	7.9400 (7.939)	19.8358 (19.835)	39.6248 (39.624)	67.2506 (67.250)	102.6356 (102.634)
	FPT	7.9400	19.8358	39.6248	67.2506	102.6355
	CPT	7.9437 (7.943)	19.8594 (19.859)	39.7188 (39.718)	67.5220 (67.522)	103.2690 (103.269)
2	SPT	7.0390	17.5840	35.1233	59.6034	90.9501
	HPT	7.0390	17.5840	35.1234	59.6037	90.9508
	FPT	7.0392	17.5853	35.1285	59.6184	91.9850
	CPT	7.0426	17.6065	35.2130	59.8621	91.5538
5	SPT	7.2606	18.1324	36.2014	61.3921	93.5999
	HPT	7.2606 (7.260)	18.1327 (18.132)	36.2025 (36.203)	61.3951 (61.395)	93.6069 (93.605)
	FPT	7.2615	18.1380	36.2236	61.4559	93.7481
	CPT	7.2657 (7.265)	18.1642 (18.164)	36.3285 (36.328)	61.7585 (61.758)	94.4542 (94.454)
10	SPT	7.4634	18.6365	37.2001	63.0673	96.1183
	HPT	7.4634 (7.462)	18.6366 (18.636)	37.2006 (37.200)	63.0687 (63.068)	96.1213 (96.120)
	FPT	7.4644	18.6427	37.2246	63.1378	96.2820
	CPT	7.4692 (7.469)	18.6731 (18.673)	37.3463 (37.346)	63.4888 (63.488)	97.1005 (97.100)

The results in parenthesis are obtained in [32].

Table 2. Critical buckling temperature change T_{cr} of FGM plate under linear temperature rise for different values of power law index k and aspect ratio a/b.

k	Theory	$a/b=1$	$a/b=2$	$a/b=3$	$a/b=4$	$a/b=5$
0	SPT	24.1789	75.3753	160.5109	279.3000	431.3459
	HPT	24.1789 (24.177)	75.3751 (75.376)	160.5102 (160.505)	279.2980 (279.297)	431.3412 (431.334)
	FPT	24.1789	75.3751	160.5102	279.2979	431.3409
	CPT	24.1982 (24.198)	75.4955 (75.495)	160.9910 (160.991)	280.6848 (280.684)	434.5767 (434.576)
1	SPT	5.5138	27.8242	64.9379	116.7498	183.1140
	HPT	5.5138 (5.513)	27.8242 (27.823)	64.9376 (64.936)	116.7490 (116.748)	183.1123 (183.110)
	FPT	5.5138	27.8242	64.9376	116.7490	183.1122
	CPT	5.5209 (5.520)	27.8683 (27.868)	65.1140 (65.114)	117.2580 (117.258)	184.3002 (184.300)
2	SPT	3.5893	22.1521	53.0271	96.1203	151.3011
	HPT	3.5893	22.1522	53.0273	96.1209	151.3023
	FPT	3.5897	22.1544	53.0363	96.1467	151.3624
	CPT	3.5956	22.1916	53.1850	96.5757	152.3637
5	SPT	3.8911	22.6047	53.7068	97.0673	152.5063
	HPT	3.8912 (3.891)	22.6052 (22.604)	53.7086 (53.710)	97.0725 (97.073)	152.5184 (152.516)
	FPT	3.8927	22.6143	53.7450	97.1771	152.7615
	CPT	3.8999 (3.899)	22.6595 (22.659)	53.9256 (53.925)	97.6980 (97.698)	153.9769 (153.977)
10	SPT	4.3653	24.1648	57.0607	102.8991	161.4674
	HPT	4.3653 (4.364)	24.1650 (24.165)	57.0615 (57.061)	102.9015 (102.901)	161.4729 (161.471)
	FPT	4.3670	24.1757	57.1041	103.0240	161.7575
	CPT	4.3757 (4.375)	24.2297 (24.229)	57.3198 (57.319)	103.6459 (103.646)	163.2080 (163.208)

The results in parenthesis are obtained in [32].

culated by CPT.

The critical buckling temperature difference t_{cr} as a function of a/b for various values of the power law index k under a uniform, linear and non-linear temperature loads is depicted in **Figure 2**. It is observed that, with increasing the plate aspect ratio a/b, the critical buckling temperature difference also increases gradually, whatever the material gradient index k is. Since the ceramic plate is weaker than the metallic one, thus the critical buckling temperature of the first plate is higher

Table 3. Critical buckling temperature change t_{cr} of FGM plate under non-linear temperature rise for different values of index k, aspect ratio a/b, and temperature exponent β $(a/h=10)$.

k	Theory	$a/b=1$			$a/b=2$			$a/b=3$		
		$\beta=2$	$\beta=5$	$\beta=10$	$\beta=2$	$\beta=5$	$\beta=10$	$\beta=2$	$\beta=5$	$\beta=10$
0	SPT	4.8414	9.6829	17.7520	11.2294	22.4589	41.1747	20.0164	40.0328	73.3935
	HPT	4.8410	9.6821	17.7505	11.2269	22.4538	41.1654	20.0066	40.0133	73.3577
	FPT	4.8408	9.6817	17.7498	11.2246	22.4492	41.1568	19.9919	39.9838	73.3037
	CPT	5.1147	10.2294	18.7540	12.8093	25.6186	46.9675	25.6336	51.2673	93.9900
1	SPT	2.1068	4.3182	8.1906	4.9517	10.1496	19.2512	8.9711	18.3880	34.8774
	HPT	2.1066	4.3179	8.1900	4.9508	10.1476	19.2475	8.9673	18.3802	34.8626
	FPT	2.1065	4.3178	8.1898	4.9499	10.1458	19.2440	8.9615	18.3684	34.8402
	CPT	2.2072	4.5241	8.5812	5.5391	11.3534	21.5346	11.0921	22.7355	43.1235
2	SPT	1.6765	3.2736	6.1232	3.9243	7.6627	14.3327	7.0655	13.7962	25.8051
	HPT	1.6766	3.2738	6.1235	3.9246	7.6633	14.3339	7.0659	13.7970	25.8066
	FPT	1.6812	3.2828	6.1404	3.9493	7.7116	14.4242	7.1433	13.9483	26.0895
	CPT	1.7627	3.4419	6.4379	4.4256	8.6417	16.1638	8.8640	17.3080	32.3737
5	SPT	1.5955	2.8485	4.9990	3.6479	6.5126	11.4292	6.3635	11.3609	19.9377
	HPT	1.5964	2.8500	5.0017	3.6521	6.5202	11.4425	6.3755	11.3822	19.9751
	FPT	1.6141	2.8816	5.0571	3.7444	6.6849	11.7317	6.6569	11.8847	20.8569
	CPT	1.7083	3.0498	5.3522	4.2885	7.6562	13.4363	8.5888	15.3337	26.9097
10	SPT	1.6766	2.8844	4.7717	3.7953	6.5293	10.8015	6.5362	11.2448	18.6022
	HPT	1.6770	2.8851	4.7728	3.7970	6.5322	10.8062	6.5402	11.2515	18.6134
	FPT	1.6974	2.9202	4.8310	3.9016	6.7122	11.1040	6.8510	11.7862	19.4980
	CPT	1.8092	3.1126	5.1492	4.5414	7.8130	12.9250	9.0951	15.6470	25.8848

Table 4. Critical buckling temperature change t_{cr} of FGM plate under non-linear temperature rise for different values of index k, aspect ratio a/b, and temperature exponent β $(a/h=5)$.

k	Theory	$a/b=1$			$a/b=2$			$a/b=3$		
		$\beta=2$	$\beta=5$	$\beta=10$	$\beta=2$	$\beta=5$	$\beta=10$	$\beta=2$	$\beta=5$	$\beta=10$
0	SPT	16.7416	33.4833	61.3861	32.8985	65.7971	120.6281	48.6540	97.3080	178.3980
	HPT	16.7353	33.4706	61.3628	32.8633	65.7266	120.4989	48.5388	97.0776	177.9756
	FPT	16.7270	33.4541	61.3325	32.7842	65.5685	120.2090	48.1978	96.3955	176.7252
	CPT	20.5039	41.0078	75.1810	51.2823	102.5646	188.0351	102.5796	205.1592	376.1253
1	SPT	7.4586	15.2878	28.9971	15.0945	30.9390	58.6835	22.9714	47.0843	89.3070
	HPT	7.4561	15.2827	28.9875	15.0800	30.9094	58.6274	22.9214	46.9819	89.1127
	FPT	7.4529	15.2762	28.9751	15.0476	30.8430	58.5014	22.7734	46.6785	88.5373
	CPT	8.8709	18.1827	34.4879	22.1983	45.4997	86.3014	44.4106	91.0281	172.6573
2	SPT	5.8880	11.4979	21.5048	11.7774	22.9970	43.0146	17.7227	34.6058	64.7282
	HPT	5.8885	11.4981	21.5065	11.7751	22.9923	43.0059	17.7018	34.5650	64.6519
	FPT	5.9430	11.6045	21.7057	11.9755	23.3838	43.7381	18.0864	35.3160	66.0566
	CPT	7.0886	13.8415	25.8898	17.7406	34.6407	64.7936	35.4938	69.3061	129.6333
5	SPT	5.3654	9.5789	16.8104	10.1426	18.1076	31.7779	14.4932	25.8748	45.4087
	HPT	5.3742	9.5945	16.8378	10.1682	18.1534	31.8582	14.5269	25.9349	45.5142
	FPT	5.5741	9.9515	17.4644	10.8794	19.4230	34.0863	15.9245	28.4301	49.8932
	CPT	6.8687	12.2627	21.5203	17.1895	30.6885	53.8566	34.3909	61.3982	107.7502
10	SPT	5.5369	9.5255	15.7580	10.2387	17.6144	29.1395	14.3554	24.6965	40.8554
	HPT	5.5400	9.5308	15.7669	10.2435	17.6226	29.1530	14.3463	24.6810	40.8297
	FPT	5.7630	9.9144	16.4014	11.0005	18.9250	31.3076	15.7723	27.1342	44.8880
	CPT	7.2736	12.5134	20.7009	18.2025	31.3150	51.8043	36.4172	62.6510	103.6433

than that of the second. For the FGM plate, t_{cr} decreases as the metallic constituent in the plate increases.

Figure 3 investigates the critical buckling temperature difference t_{cr} of homogeneous and FG plates versus the side-to-thickness ratio a/h under various types of temperature loads. **Figure 4** gives similar for FG plates versus the aspect ratio a/b. The buckling temperature of the homogeneous plate is considerably higher than

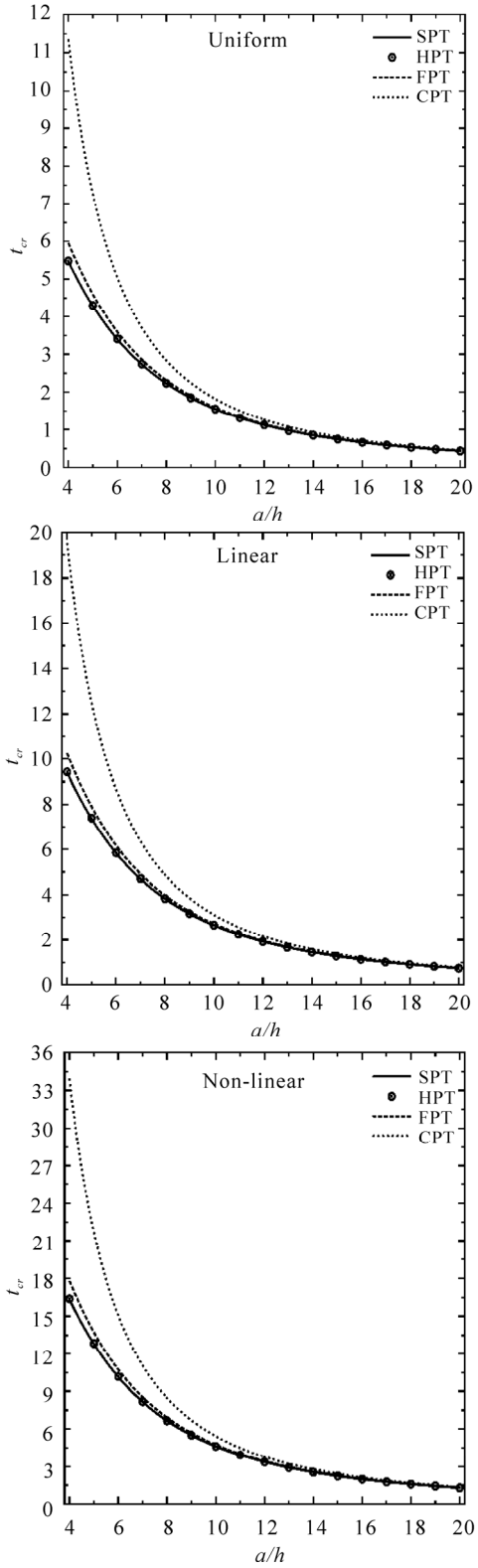

Figure 1. Critical buckling temperature difference t_{cr} due to uniform, linear and non-linear temperature rise across the thickness versus the side-to-thickness ratio a/h.

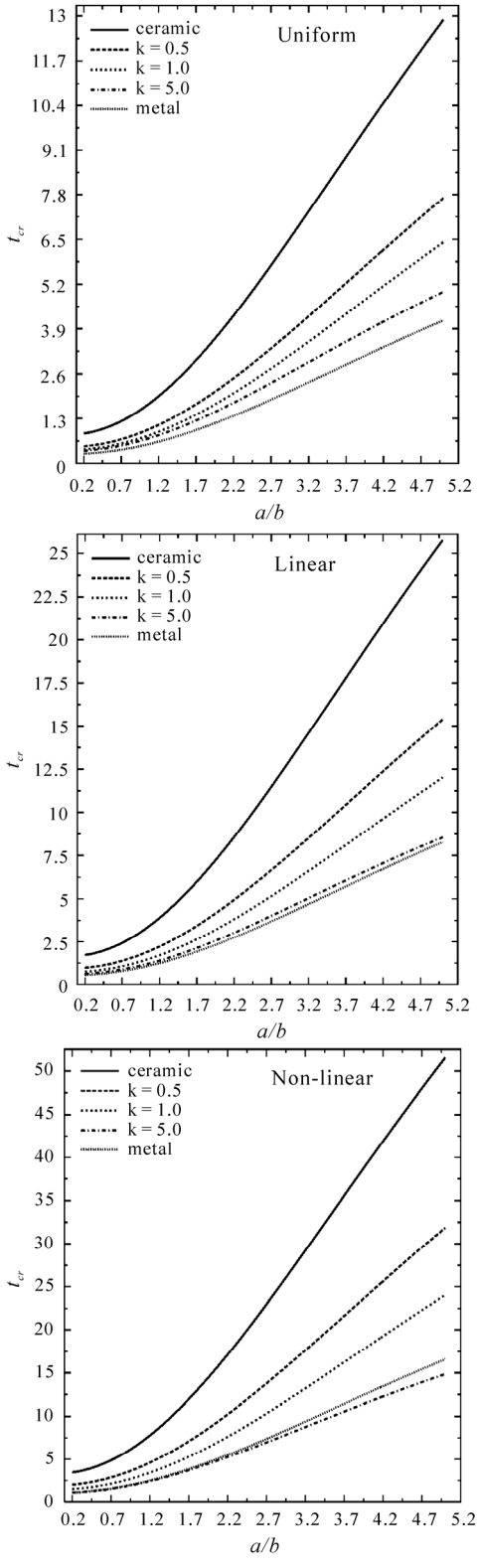

Figure 2. Critical buckling temperature difference t_{cr} due to uniform, linear and non-linear temperature rise across the thickness versus the aspect ratio a/b.

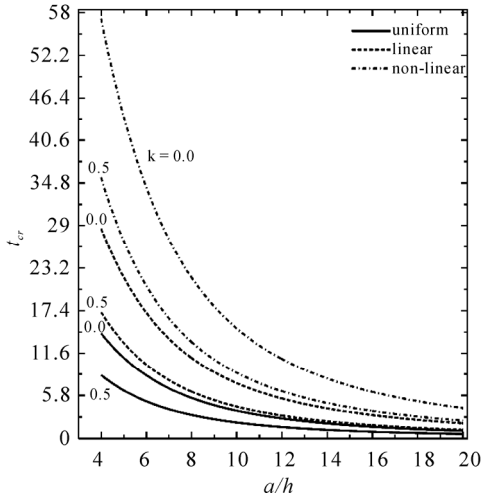

Figure 3. Critical buckling temperature difference t_{cr} due to uniform, linear and non-linear temperature rise across the thickness versus the side-to-thickness ratio a/h.

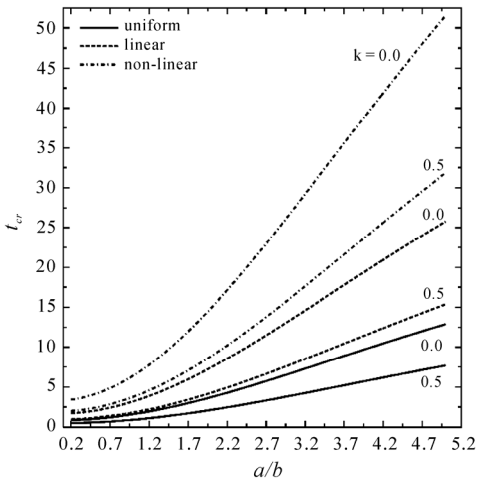

Figure 4. Critical buckling temperature difference t_{cr} due to uniform, linear and non-linear temperature rise across the thickness versus the aspect ratio a/b.

that for the FGM one, especially for the comparatively thicker plates. Again, because of the thicker plates are stronger than the thinner ones, thus the critical buckling temperature of the first type is higher than that of the second one. Note that t_{cr} of the plate under uniform temperature rise is smaller than that of the plate under linear temperature rise and the latter is smaller than that of the plate under non-linear temperature rise.

6. CONCLUSIONS

The thermal buckling analysis for ceramic-metal FG plates under uniform, linear and nonlinear thermal loading through the thickness is investigated in this paper. The constituent materials are graded from the ceramic surface to the metallic surface according to the power law variation. The SPT is used to deduce the equilibrium and stability equations for a simply supported functionally graded rectangular plate under thermal loading. The results obtained using SPT are compared with those obtained using HPT, FPT and CPT; and compared with published ones. The numerical results of critical buckling temperature difference using SPT are very close to those of HPT and the two theories have similar trends for all cases of loading. The critical buckling temperature difference is proportional to the plate aspect ratio. The thicker plates need a temperature to buckle higher than that the thinner plates need it. The critical buckling temperature differences of functionally graded plates are generally lower than the corresponding ones for homogeneous ceramic plates.

7. ACKNOWLEDGEMENTS

The investigators would like to express their appreciation to the Deanship of Scientific Research at King AbdulAziz University for its financial support of this study, Grant No. 3-038/429.

REFERENCES

[1] Koizumi, M. (1997) FGM activities in Japan. *Composites Part B*: *Engineering*, **28(1-2)**, 1-4.

[2] Bhangale, R.K. and Ganesan, N. (2005) A linear thermoelastic buckling behavior of functionally graded hemispherical shell with a cut-out at apex in thermal environment. *International Journal of Structural Stability and Dynamics*, **5(2)**, 185-215.

[3] Javaheri, R. and Eslami, M.R. (2002) Buckling of functionally graded plates under in-plane compressive loading. *ZAMM – Journal of Applied Mathematics and Mechanics*, **82(4)**, 277-283.

[4] Chung, Y.-L. and Chang, H.-X. (2008) Mechanical behavior of rectangular plates with functionally graded coefficient of thermal expansion subjected to thermal loading. *Journal of Thermal Stresses*, **31(4)**, 368-388.

[5] Praveen, G.N. and Reddy, J.N. (1998) Nonlinear transient thermoelastic analysis of functionally graded ceramic-metal plates. *International Journal of Solids and Structures*, **35(33)**, 4457-4476.

[6] Reddy, J.N. (2000) Analysis of functionally graded plates. *International Journal for Numerical Methods in Engineering*, **47(1-3)**, 663-684.

[7] Amini, M.H., Soleimani, M. and Rastgoo, A. (2009) Three-dimensional free vibration analysis of functionally graded material plates resting on an elastic foundation. *Smart Materials and Structures*, **18(8)**, 1-9.

[8] Sladek, J., Sladek, V., Hellmich, Ch. and Eberhardsteiner, J. (2007) Analysis of thick functionally graded plates by local integral equation method. *Communications in Numerical Methods in Engineering*, **23(8)**, 733-754.

[9] Kim, J.-H. and Paulino, G.H. (2002) Finite element evaluation of mixed mode stress intensity factors in functionally graded materials. *International Journal for Numerical Methods in Engineering*, **53(8)**, 1903-1935.

[10] Altenbach, H. and Eremeyev, V.A. (2008) Analysis of the viscoelastic behavior of plates made of functionally graded materials. *ZAMM – Journal of Applied Mathematics and Mechanics*, **88(5)**, 332-341.

[11] Ovesy, H.R. and Ghannadpour, S.A.M. (2007) Large deflection finite strip analysis of functionally graded plates under pressure loads. *International Journal of Structural Stability and Dynamics*, **7(2)**, 193-211.

[12] Han, X., Liu, G.R. and Lam, K.Y. (2001) Transient waves in plates of functionally graded materials. *International Journal for Numerical Methods in Engineering*, **52(8)**, 851-865.

[13] Zenkour, A.M. (2007) Benchmark trigonometric and 3-D elasticity solutions for an exponentially graded thick rectangular plate. *Archive of Applied Mechanics*, **77(4)**, 197-214.

[14] Zenkour, A.M. (2005) A comprehensive analysis of functionally graded sandwich plates: Part 1-Deflection and stresses. *International Journal of Solids and Structures*, **42(18-19)**, 5224-5242.

[15] Zenkour, A.M. (2005) A comprehensive analysis of functionally graded sandwich plates: Part 2-Buckling and free vibration. *International Journal of Solids and Structures*, **42(18-19)**, 5243-5258.

[16] Zenkour, A.M. (2005) On vibration of functionally graded plates according to a refined trigonometric plate theory. *International Journal of Structural Stability and Dynamics*, **5(2)**, 279-297.

[17] Aliaga, J.W. and Reddy, J.N. (2004) Nonlinear thermoelastic analysis of functionally graded plates using the third-order shear deformation theory. *International Journal of Computational Engineering Science*, **5(4)**, 753-779.

[18] Arciniega, R.A. and Reddy, J.N. (2007) Large deformation analysis of functionally graded shells. *International Journal of Solids and Structures*, **44(6)**, 2036-2052.

[19] Kadoli, R., Akhtar, K. and Ganesan, N. (2008) Static analysis of functionally graded beams using higher order shear deformation theory. *Applied Mathematical Modelling*, **32(12)**, 2509-2525.

[20] Sina, S.A., Navazi, H.M. and Haddadpour, H. (2009) An analytical method for free vibration analysis of functionally graded beams. *Materials & Design*, **30(3)**, 741-747.

[21] Zhao, X., Lee, Y.Y. and Liew, K.M. (2009) Mechanical and thermal buckling analysis of functionally graded plates. Composite Structures, **90(2)**, 161-171.

[22] Matsunaga, H. (2009) Thermal buckling of functionally graded plates according to a 2D higher-order deformation theory. *Composite Structures*, **90(1)**, 76-86.

[23] Morimoto, T., Tanigawa, Y. and Kawamura, R. (2006) Thermal buckling of functionally graded rectangular plates subjected to partial heating. *International Journal of Mechanical Sciences*, **48(9)**, 926-937.

[24] Shariat, B.A.S. and Eslami, M.R. (2006) Thermal buckling of imperfect functionally graded plates. *International Journal of Solids and Structures*, **43(14-15)**, 4082-4096.

[25] Ganapathi, M. and Prakash, T. (2006) Thermal buckling of simply supported functionally graded skew plates. *Composite Structures*, **74(2)**, 247-250.

[26] Lanhe, W. (2004) Thermal buckling of a simply supported moderately thick rectangular FGM plate. *Composite Structures*, **64(2)**, 211-218.

[27] Najafizadeh, M.M. and Heydari, H.R. (2004) Thermal buckling of functionally graded circular plates based on higher order shear deformation plate theory. *European Journal of Mechanics A/Solids*, **23(6)**, 1085-1100.

[28] Babu, C.S. and Kant, T. (2000) Refined higher order finite element models for thermal buckling of laminated composite and sandwich plates. *Journal of Thermal Stresses*, **23(2)**, 111-130.

[29] Zenkour, A.M. (2006) Generalized shear deformation theory for bending analysis of functionally graded plates. *Applied Mathematical Modelling*, **30(1)**, 67-84.

[30] Zenkour, A.M. (2004) Buckling of fiber-reinforced viscoelastic composite plates using various plate theories. *Journal of Engineering Mathematics*, **50(1)**, 75-93.

[31] Zenkour, A.M. (2004) Thermal effects on the bending response of fiber-reinforced viscoelastic composite plates using a sinusoidal shear deformation theory. *Acta Mechanica*, **171(3-4)**, 171-187.

[32] Javaheri, R. and Eslami, M.R. (2002) Thermal buckling of functionally graded plates based on higher order theory. *Journal of Thermal Stresses*, **25(7)**, 603-625.